A Planar MICS Band Antenna Combined With a Body Channel Communication Electrode for Body Sensor Network

Namjun Cho, *Student Member, IEEE*, Taehwan Roh, *Student Member, IEEE*, Joonsung Bae, *Student Member, IEEE*, and Hoi-Jun Yoo, *Fellow, IEEE*

***Abstract*—A 2.5 × 1.8 cm^2 medical implant communication service band antenna is combined with an electrode for body channel communication. The proposed design enables a body sensor network controller to communicate with health-care devices located on and inside a patient's body. The spiral microstrip antenna with its radiating body and ground plane placed side-by-side has the thickness of 2 mm and can be attached to human skin conveniently. The propagation loss of the body channel is measured when the proposed antenna is used as the skin interface for BCC in the 10–70-MHz band, and the results are compared with the cases of Ag/AgCl and circular dry electrodes. The equivalent-circuit model of the antenna as the electrode is also derived from the measured impedance characteristics. The *LC* resonance structure to drive the on-body antenna with its capacitance increased due to the skin contact reduces the power consumption of the TX buffer by >50%. The S_{11}-parameter of the on-body antenna, its radiation pattern, and the signal loss inside the human body are investigated.**

***Index Terms*—Body channel communication (BCC), body sensor network, electrode, medical implant communication service (MICS) band antenna, planar spiral antenna.**

I. Introduction

With THE increasing number of implantable health-care devices such as pacemakers, neurostimulators, and retinal prostheses, their wireless communication with an external controller is gaining attention. The inductive coupling technique widely adopted in primitive designs of the implantable devices is not appropriate to the recent biomedical systems as they become highly programmable and miniaturized [1]. In order to improve the limited data rate and communication range of the near-field inductive coupling, the Federal Communications Commission (FCC) allocated the 402–405-MHz medical implant communication service (MICS) band [2]. Although far-field communication using a MICS band radio increases patient mobility and data rate [3], [4], the stringent TX power regulation claimed by the FCC is the main obstacle to the construction of the ubiquitous health care network, which needs to cover at least a 10-m area around a patient. Since the 402–405-MHz band is shared with meteorological and earth exploration satellites, the effective isotropic radiation power (EIRP) from a MICS radio is limited to only −16 dBm to generate no interference with the primary users [2]. This low emission power experiences huge propagation loss through the air channel and the conductive human tissue, as shown in Fig. 1(a) [4]. As a result, communication distance between an implanted device and an outside controller is confined to 2 m, and the sensitivity of −90 dBm is required in the implanted radio, causing its large power consumption.

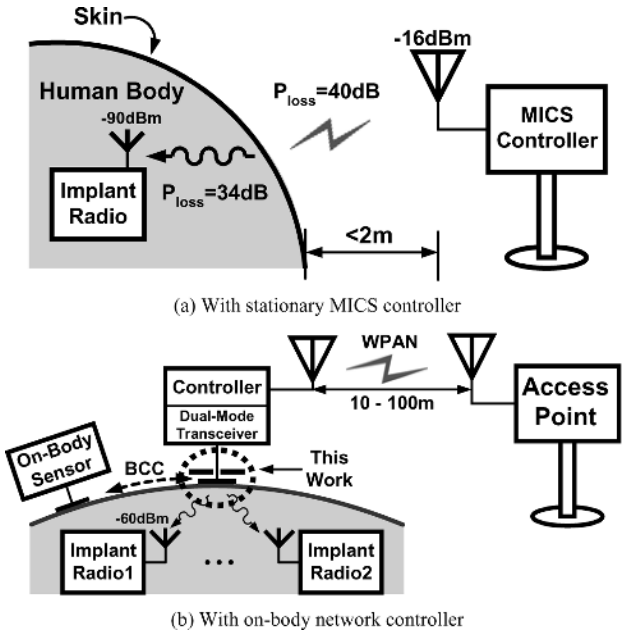

Fig. 1. Wireless body sensor network using MICS band.

Fig. 1(b) shows a new type of body-sensor network with its controller located on the human body [5]. This configuration can resolve the short-range issue pointed out in Fig. 1(a) by incorporating the MICS with the wireless personal area network (WPAN) such as Bluetooth and ultra-wideband (UWB). Owing to removal of the air channel, the sensitivity of the implanted MICS radio can be raised to −60 dBm, allowing its design to be simplified for ultra-low-power consumption [6], [7]. The on-body network controller stores medical data collected from the multiple implanted units temporarily and delivers them to the remote access point using the WPAN technique that operates in 10–100-m distance. Moreover, the controller can communicate with wearable health monitoring sensors using body channel communication (BCC) [8]. BCC is a new type of communication, which uses the human body itself as a

Manuscript received February 20, 2009; revised June 23, 2009. First published September 25, 2009; current version published October 14, 2009.

The authors are with the Department of Electrical Engineering, Korea Advanced Institute of Science and Technology (KAIST), Daejeon 305-701, Korea (e-mail: cho.namjun@gmail.com; noradi@eeinfo.kaist.ac.kr; joonsung@eeinfo.kaist.ac.kr; hjyoo@ee.kaist.ac.kr).

Digital Object Identifier 10.1109/TMTT.2009.2029952

transmission medium. Since BCC uses a frequency band less than 100 MHz without requiring a large antenna, this technique is actively studied as a low-power and interference-free method connecting medical sensors on a patient [9]. In order to transfer data through the body channel, a BCC transmitter (TX) applies voltage signal between its ground plane and the electrode attached on human skin. As the TX and receiver (RX) are coupled to each other by parasitic capacitance between their ground planes, the RX can detect data by sensing a feeble change of electric field incurred by the voltage swing in the TX side. The electrode is the component that transforms the electric field formed around the RX to the voltage signal. As shown in Fig. 1(b), the MICS band antenna attached on the skin also functions as the BCC electrode, and the controller transceiver can be configured to operate in the MICS and BCC modes [5].

This paper deals with the on-body antenna combined with the BCC electrode for the dual-mode communication. Previously, most of the MICS band antennas are designed to be implanted inside the human body, and not optimized for the on-body environment [10], [11]. Section II discusses design constraints of the dual-mode antenna and its geometry to meet the requirements. The S_{11}-parameter of the antenna and the loss of the signal radiated inside the body are investigated. Section III focuses on the characteristics of the antenna as the electrode, and its equivalent-circuit model is derived. Finally, a low-power BCC buffer using *LC* series resonance is proposed to drive the large capacitance of the on-body antenna.

II. Planar MICS Band Antenna as the BCC Electrode

A. Design of the MICS Antenna Combined With an Electrode

The proposed on-body antenna needs special considerations in its design to support the dual-mode operation. As an electrode for BCC, the radiating body of the antenna should be attached on skin securely to minimize the contact impedance at the signal interface. Due to the 0.1–1-S/m conductivity (σ) and 40–60 relative permittivity (ε_r) of the skin, the resonant frequency of the antenna shifts and its radiation efficiency degrades much. In addition, the multilayered structure of the human tissue makes analytical design of the on-body antenna complicated. The small and planar geometry of the antenna is desirable to make it worn by patients with comfort. However, the low-profile designs such as loop and planar inverted F [10], [12] are prohibited because their signal and ground pins are shorted in $<$100-MHz frequency bands for BCC.

Fig. 2 presents the antenna structure that satisfies the constraints mentioned above. The design is obtained by modifying the spiral microstrip antenna [10] of an implanted biotelemetry. The ground pin on the radiating body of the conventional antenna is eliminated to make the signal and ground pins open at the BCC frequency bands. Instead, the 3×4 cm^2 ground plane is placed 1.5 mm below the radiating body. The central axes of the two plates are separated by 28.8 mm. The resonant frequency of the antenna is lowered to 650 MHz with the small body area of 2.5×1.8 cm^2 and 1.8-mm thickness because the fringing effect dominant in the structure of Fig. 2(b) increases the effective antenna size. Arranging the radiating body and the ground plane side-by-side is also advantageous for BCC. When

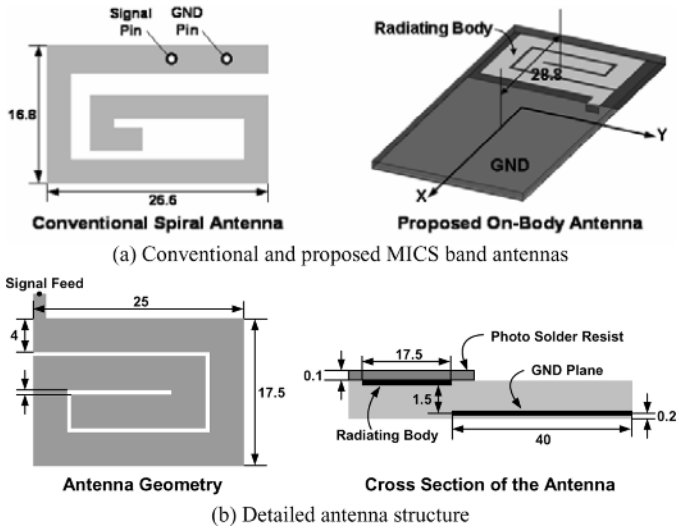

Fig. 2. Proposed MICS band antenna combined with BCC electrode (all dimensions are in millimeters).

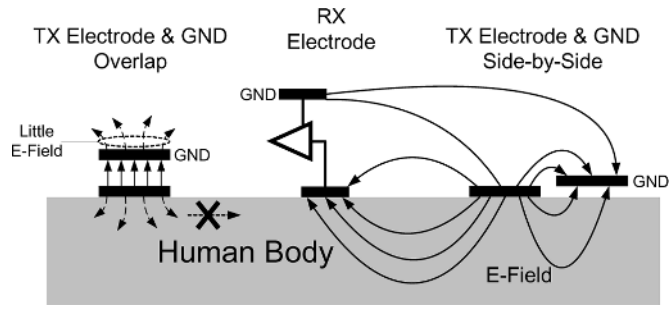

Fig. 3. Electric fields formed around the BCC electrode.

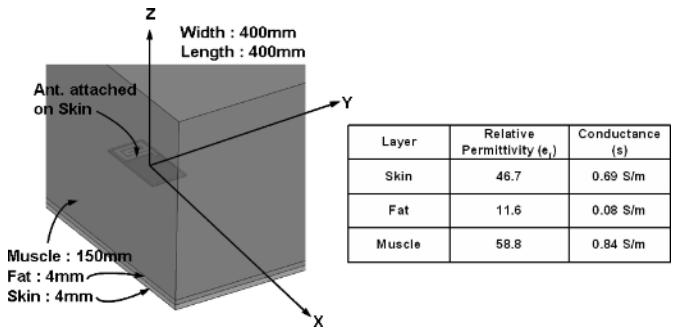

Layer	Relative Permittivity (ε_r)	Conductance (s)
Skin	46.7	0.69 S/m
Fat	11.6	0.08 S/m
Muscle	58.8	0.84 S/m

Fig. 4. Antenna simulation setup.

the two plates do not overlap each other, as shown in Fig. 3, strong electric fields can be radiated from the TX electrode and coupled to the RX electrode and ground, making a larger voltage signal detected by the RX circuitry. The 3×4 cm^2 area for the ground plane does not increase overall system size because a dual-mode transceiver, oscillator, and passive circuits can be placed on it [5]. Therefore, the actual area overhead of the proposed antenna is 2.5×1.8 cm^2. Fig. 2(b) shows the detailed structure of the spiral radiating body tuned to get the best return loss and antenna efficiency. The design parameters including the number of spiral turns, line width, and line space are optimized through electromagnetic (EM) field simulations. For the simulation, the antenna model is placed on a multilayered box, which emulates human tissue, as shown in Fig. 4. Since

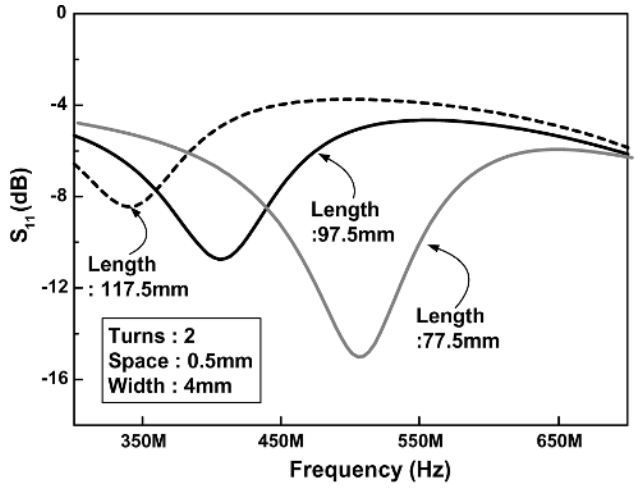

(a) Line length changed

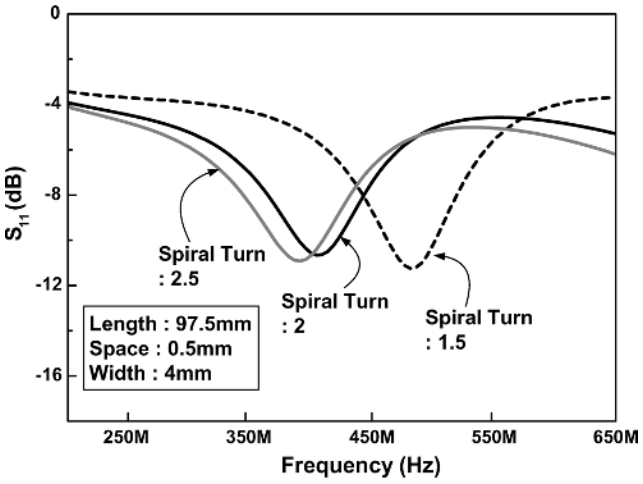

(b) Number of spiral turns changed

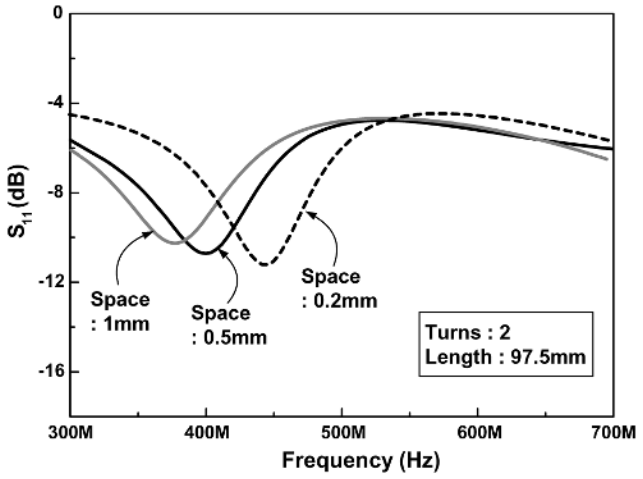

(c) Line space changed

Fig. 5. Simulated return losses of the proposed antenna.

the antenna is expected to be attached on the chest or stomach of a patient, the simple rectangular structure can approximate the human body with enough accuracy and reduced simulation time. The $400 \times 400 \times 158$ mm^3 box consists of skin, fat, and muscle layers, which are used in [11] for a human body model. Finally, the radiating body, which makes direct contact with the

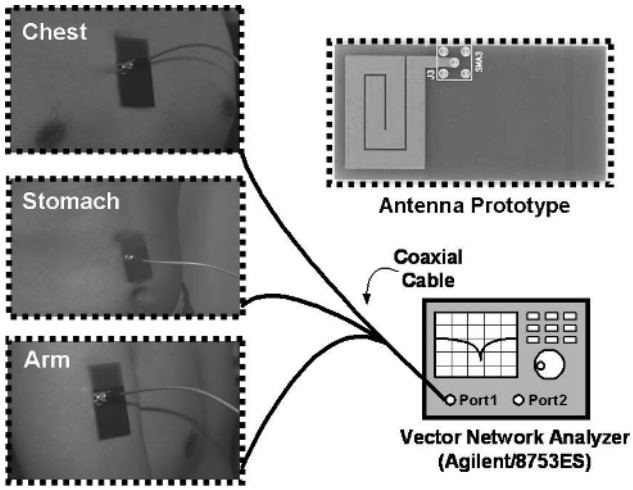

Fig. 6. Experimental setup for S_{11} measurements.

skin, is covered with a 100-μm photo solder resist (PSR) layer to prevent severe degradation of the antenna matching performance. Fig. 5(a) shows the simulated return loss of the antenna as the line length changes. The spiral antenna can be regarded as a monopole antenna, which is folded on a planar circuit board for a small area. Hence, the resonant frequency of the antenna mainly depends on its length. The increasing number of spiral turns reduces the resonant frequency, as shown in Fig. 5(b). Beyond the two turns, however, the resonant frequency does not change much. The return loss of the antenna degrades as the line length increases while the number of spiral turns is not so related. Therefore, the line length is decided as the minimum with the two spiral turns fixed to give the desired resonant frequency. The magnitude of the return loss is tuned by changing the line space and linewidth. Fig. 5(c) is the return loss simulated with various line spaces. If the size of the antenna is kept constant, the linewidth is determined automatically. As the space becomes narrower, the S_{11} drop is deeper at the resonant frequency. However, when the radiation efficiency is taken into consideration, the space of 0.5 mm is preferred to 0.2 mm.

B. Antenna Characteristics

Fig. 6 shows the experimental setup for return-loss measurement of the on-body antenna. A port of the vector network analyzer is extended by a coaxial cable and the antenna under test is connected to the cable by a subminiature A (SMA) connector. The return losses of the antenna measured at various locations on the human subject are presented in Fig. 7. As expected, the resonant frequency of the antenna is decreased from 790 MHz in the air [see Fig. 7(a)] to around 400 MHz on the body [see Fig. 7(b)] due to the high electrical permittivity of the human tissue. According to the graph, the antenna return losses on the stomach and the arm correspond to the simulation data better than those on the chest. It may be because the three-layer box used for the simulation does not include a bone layer, which is the significant part of the chest. Another observation from the measurements is that the -10-dB bandwidth of the antenna is increased three times and the return loss is less than -4 dB even at nonresonant frequencies when the antenna is attached on the

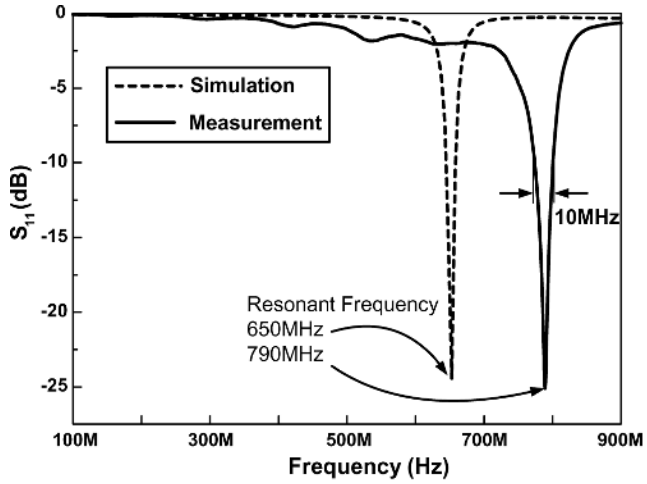

(a) Antenna in air

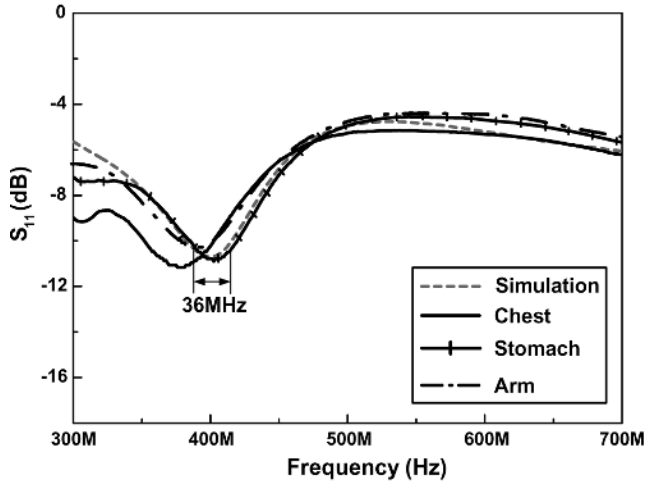

(b) Antenna on the human body

Fig. 7. Measured S_{11}-parameters of the on-body antenna.

skin. These wideband characteristics come from the body conductivity. The impedance (Z_{ANT}) of the on-body antenna can be represented as

$$Z_{\mathrm{ANT}} = R_L + R_R + R_B + jX_F \tag{1}$$

where X_F is the antenna reactance, and R_L and R_R are the resistances related to the antenna loss and radiation [13]. The loss term due to the body conductivity is also added as R_B. At the frequencies away from the antenna resonance, R_L and R_R are almost zero, but the body conductivity of 0.1–1 S/m keeps the R_B around 20 Ω over the wide frequency range. Therefore, we should not conclude that the antenna on the human body can radiate more power around it at the nonresonant frequencies. To verify this qualitative explanation, an antenna simulation is conducted with the settings described in Section II-A, except that the conductivity of each tissue layer used in the previous simulation is made zero. As shown in Fig. 8, the antenna bandwidth does not widen while the resonant frequency is still near 400 MHz. The irregular peaks in the S_{11} curve are due to reflection of the microwaves radiated into the rectangular box at its boundary. When the thickness of the muscle layer is reduced to less than 30 mm, the peaks disappear. Fig. 9 shows the simulated far-field radiation pattern of the antenna.

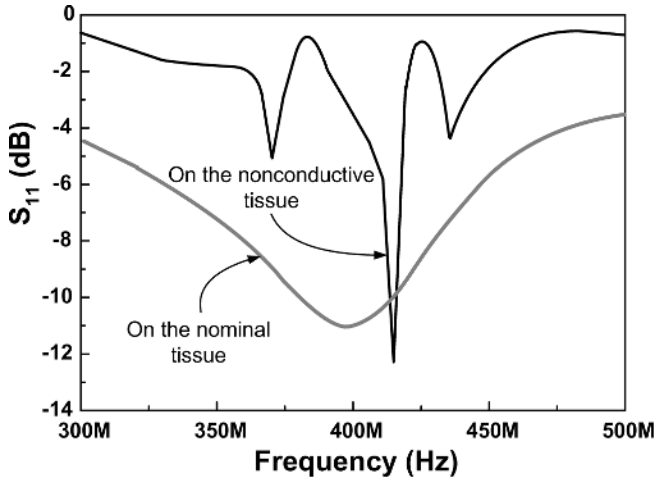

Fig. 8. S_{11}-parameter of the antenna on the nonconductive human tissue.

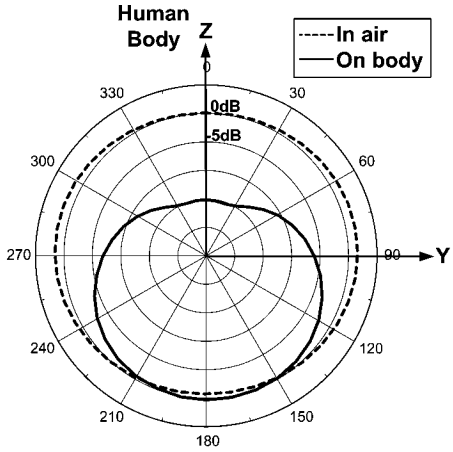

(a) Y-Z

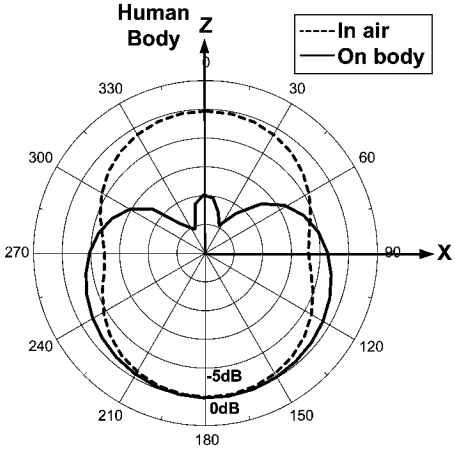

(b) X-Z

Fig. 9. Simulated radiation pattern of the antenna.

It can be easily found that the field patterns symmetric with respect to x and y axes (Fig. 4) are severely distorted when it is located on the human body. The radiation amount toward the human body is decreased by more than 15 dB since the conductive human tissue blocks most of the signal radiated from the antenna. Since our main interest is how much the signal attenuates propagating the lossy human body, the path-loss measurements inside a human phantom are performed. The phantom of Fig. 10 is enclosed by 5 mm polyvinyl chloride

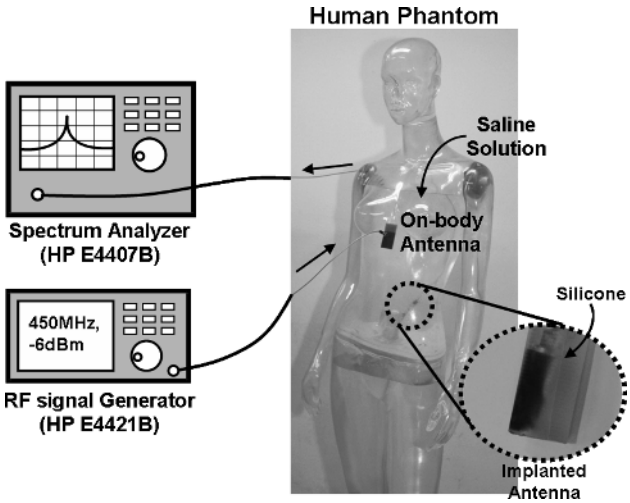

Fig. 10. Experimental setup for measuring path loss inside human phantom.

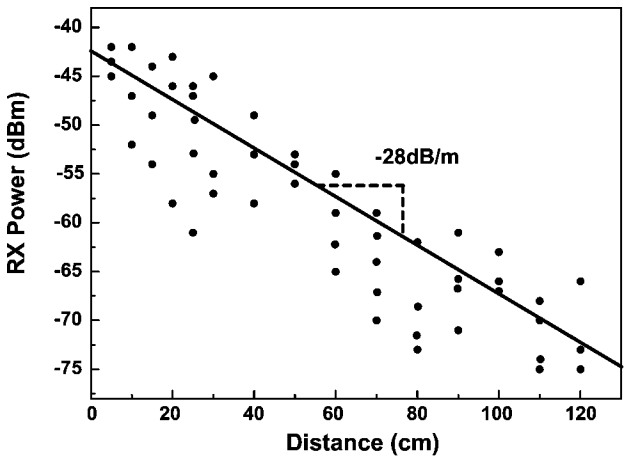

Fig. 11. RX power versus distance inside the human phantom.

(PVC) and filled with the saline solution, which shows the electrical characteristics ($\sigma = 1.2$ S/m, $\varepsilon_r = 80$) similar to those of the internal human organs [14]. This model has the accurate geometry of a 170-cm female body, and hence, the effects of scattering and reflection on the body surface can be taken into account. The helical antenna is coated with silicone to be inserted into the saline solution, and the proposed antenna is located on the phantom chest. Due to the 5-mm PVC, the resonant frequency of the antenna slightly shifts to 450 MHz. Therefore, this frequency is used for the experiments instead of 400 MHz. The TX power applied to the antenna is set to -6 dBm. Since the antenna efficiency is 10% on human skin, the radiation power is -16 dBm, which is the maximum value allowed by the FCC [2]. At least three different locations for a given channel length are selected inside the human phantom and the RX power measured at each location is displayed in Fig. 11. The RX power degrades according to distance between the two antennas with a -26-dB/m rate. However, the minimum power level is still -75 dBm, which is larger than the sensitivity of the most ultra-low-power radios consuming less than 1 mW [6], [7]. If the implanted helical antenna is optimized for the environment inside the body, the RX power is expected to be higher.

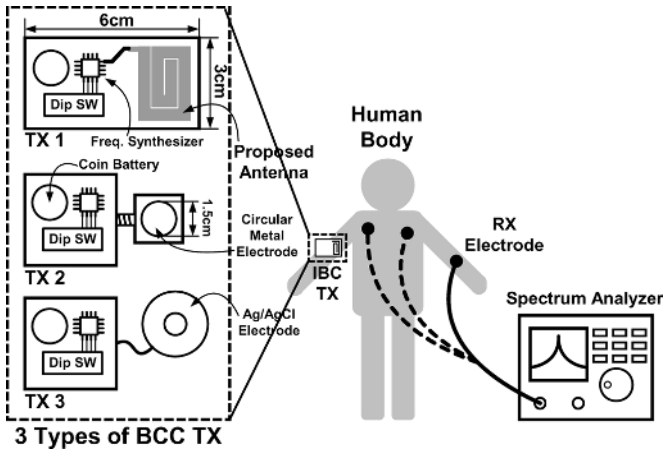

Fig. 12. Experimental setup for measuring path loss of the body channel.

III. BCC Electrode

The electrode for BCC should satisfy two conditions. The first one is having the low contact impedance at the skin–electrode interface, and the other one is giving the small capacitive load to the BCC TX for its low power consumption. For the low contact resistance, most of the BCC transceivers use an Ag/AgCl electrode or a bare metal electrode, which is directly attached on the skin [9], [15]. However, as the radiating metal of the proposed antenna is covered with the protective 100-μm PSR layer, capacitive coupling between the antenna and the skin increases the contact impedance and affects the channel characteristics of BCC. In this study, the path loss of the body channel when the antenna is used as the electrode is compared with the Ag/AgCl and the circular metal electrode cases. The load impedance of the antenna is calculated from the measured S_{11}-parameter, and the equivalent-circuit model is derived. The *LC* resonance buffer driving the large capacitance of the antenna is also proposed for the low-power BCC.

A. Path-Loss Measurement of Body Channel

The experimental setup to measure the path loss of the body channel is shown in Fig. 12 [8]. The 3×6 cm^2 TX boards consisting of a coin battery and a frequency synthesizer programmable with a wide tuning range use three types of electrode—an Ag/AgCl electrode, a circular metal electrode, and the proposed antenna. The frequency range of the measurement is 10–70 MHz, which is decided as the optimal band for BCC in the previous channel study [8]. The voltage swing at the TX is 3 V. The RX electrode is a circular metal with 1.5-cm diameter and connected to the spectrum analyzer by a coaxial cable. The same RX electrode is used for all channel measurements to detect the electric field that appears between the body and RX ground under the same condition. The strength of the capacitive return path between TX and RX grounds affects propagation loss of BCC significantly. The ground area of each TX system is maintained as 3×4 cm^2. Under the experimental setup, the case of the spectrum analyzer is treated as the RX ground. Hence, the signal magnitude measured by the spectrum analyzer is expected to be larger compared with the real situation where the

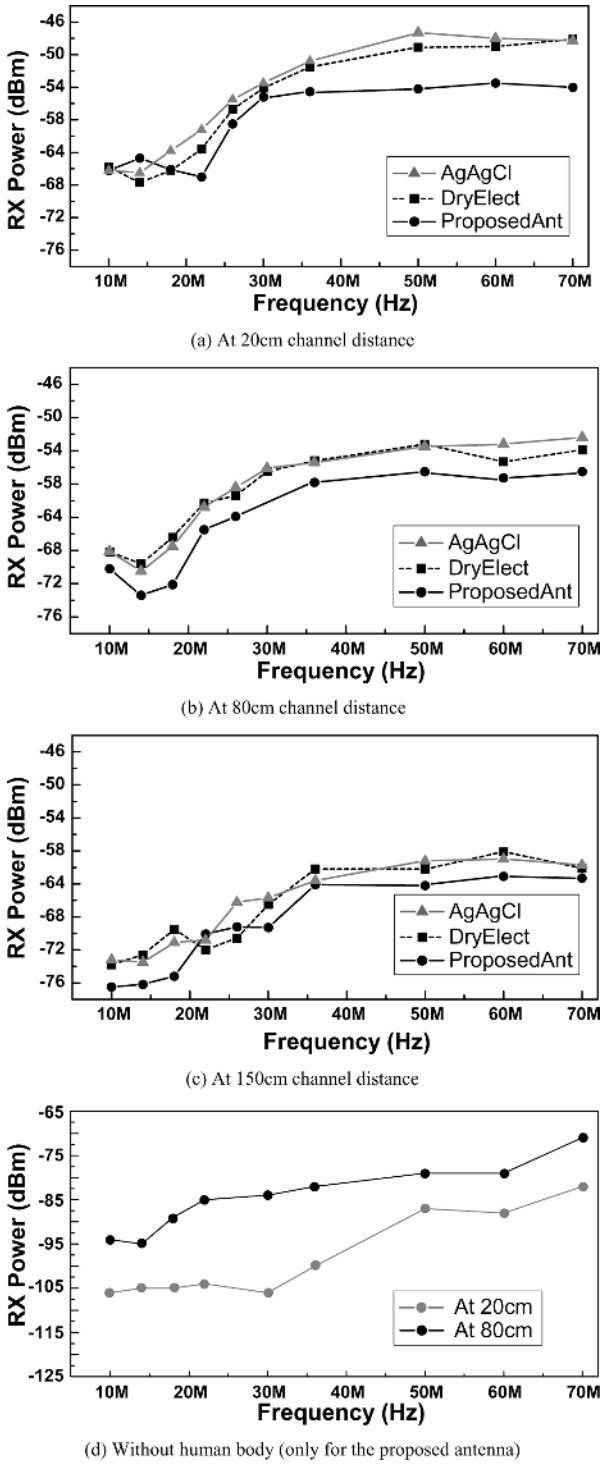

(a) At 20cm channel distance

(b) At 80cm channel distance

(c) At 150cm channel distance

(d) Without human body (only for the proposed antenna)

Fig. 13. RX powers measured through the human body.

RX is also made portable. However, this discrepancy can be ignored because the main objective of this experiment is relative comparison among the three different types of electrodes. The location of the TX board is fixed on the right arm of the human subject. The RX signal power through the body is measured at 0.2-, 0.8-, and 1.5-m distances between the TX and RX electrodes. Fig. 13 shows that the electrode type does not affect the overall shape of the RX power curve. As expected, the on-body antenna covered with the protective layer shows the largest path loss through the human body because it has the highest contact impedance than the other two electrodes. However, the RX power difference is less than 5 dB over the entire ranges of the frequency and distance. This channel degradation is affordable to be compensated by increasing the voltage swing at the TX side, or a special sensing device such as an electrooptic crystal can be used to detect the weak electric signal at the RX side [16]. At the 1.5-m channel length, the RX power level does not depend on the types of the electrode since the impedance of the body channel becomes much larger than the contact impedance. In Fig. 13(d), the propagation loss between TX and RX is additionally presented when there is no human body. From the result, it is apparent that the proposed antenna operates as an electrode rather than an antenna in the 10–70-MHz frequency range. Owing to the human body, the coupling strength between the TX and RX is greatly enhanced. At least 25-dB gain in the transmission coefficient is observed by the body coupling.

B. Equivalent-Circuit Model of the Antenna

Increasing the TX voltage swing is an attractive solution to compensate the channel loss due to the contact impedance of the proposed antenna. However, the amplitude of the TX signal affects the power consumption of the BCC transceiver significantly because of $P = CV^2 f$, where P is the power required to drive the load capacitance C with the rectangular pulse signal having the V amplitude and the f frequency. With the V and f values optimized for BCC [8], the only way to reduce the power consumption is minimizing the load capacitance of the antenna. Fig. 14 shows the real and imaginary parts of the antenna impedance (Z_{ANT}) calculated using the measured S_{11}-parameters and the conversion equation $-Z_{\mathrm{ANT}} = 50(1 + S_{11})/(1 - S_{11})$. In the 25–100 MHz, the antenna is regarded as a capacitor since the sign of the antenna reactance is negative and its magnitude is inversely proportional to frequency. Without the skin contact, the impedance curve of the antenna corresponds well to that of the 3.5-pF capacitor. However, the magnitude of the antenna reactance decreases significantly and the resistance increases when it is attached on the skin. The 0.1–1-S/m conductivity and the 40–60 relative permittivity of the human body contribute to the capacitance and resistance increments of the antenna by making the conductive and displacement current channels between the radiating body and the ground plane, as shown on the top of Fig. 15. The equivalent circuit of Fig. 15 models the antenna–body–ground interface electrically. C_1 represents the capacitive coupling between the antenna and ground through the air. C_2 and C_3 are the capacitances at the antenna–skin and the ground–skin interfaces. The R_B and C_B parallel network models the conductive and displacement current channel through the human body. The impedance curve of the equivalent circuit is also displayed in Fig. 14 to verify the accuracy of the model. Even if the effect of R_B is ignored, the capacitance of the antenna is increased by $C_2 C_B C_3 = 7.5$ pF due to the skin contact. To drive the large capacitor load with low operating power, a 230-nH inductor is inserted in the signal path from the BCC TX buffer to the antenna (Fig. 16). At the series resonance of the inductor and the capacitive antenna, the buffer only needs to compensate the resistive loss of the resonator to drive the antenna. In addition,

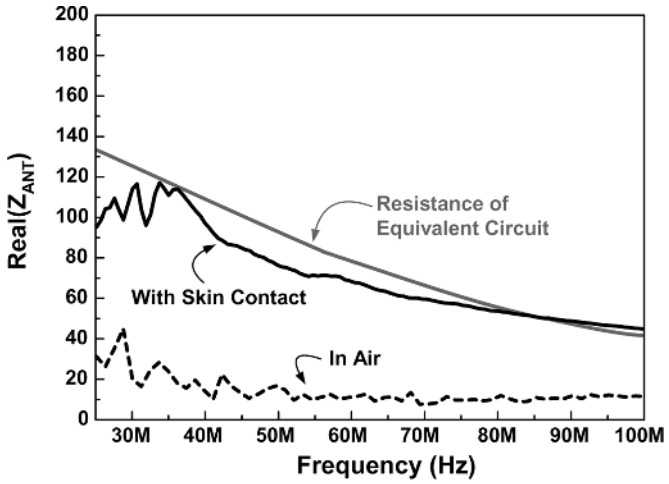

(a) Real part of the antenna impedance

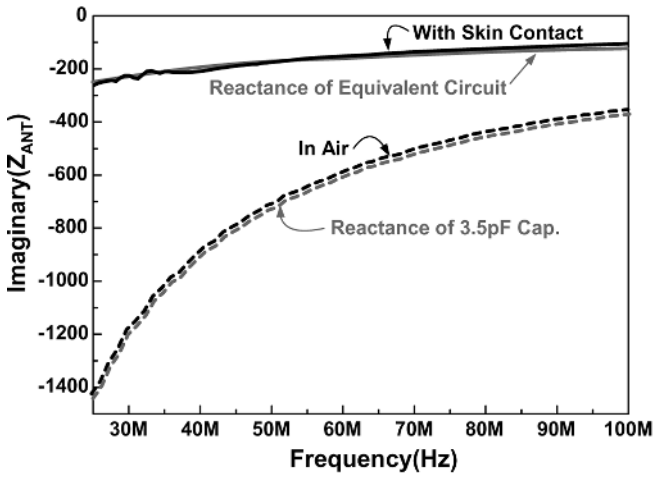

(b) Imaginary part of the antenna impedance

Fig. 14. Antenna impedance curve.

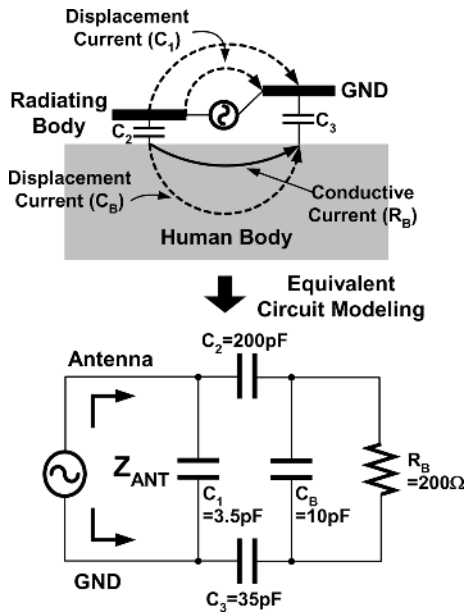

Fig. 15. Equivalent-circuit model of the antenna as an electrode.

the swing level of the signal applied to the antenna can be amplified by 8 dB even though the resistive component of the antenna degrades the Q factor of the resonator to 5. The

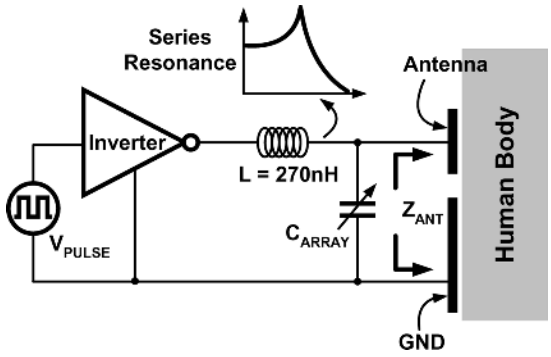

Fig. 16. *LC* resonance TX buffer.

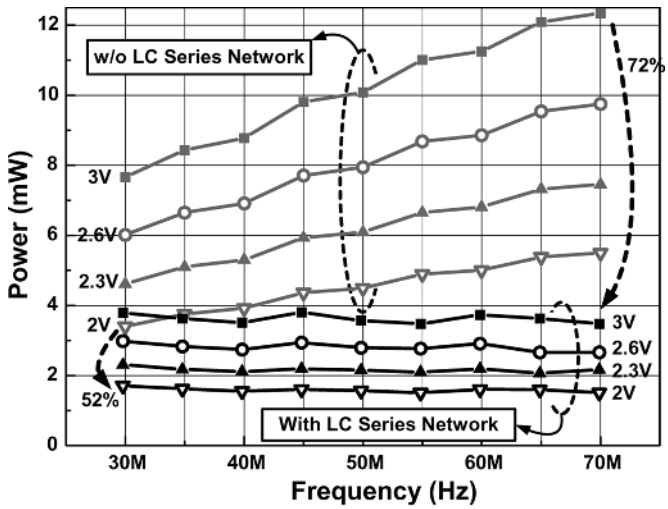

Fig. 17. Power reduction by the *LC* resonance.

5-bit programmable capacitor array is connected in parallel with the antenna to adjust the resonant frequency of the *LC* series network to the input frequency. Fig. 17 shows the power reduction by the *LC* resonance. For the TX buffer driving the on-body antenna directly, the power consumption increases in proportion to the frequency and the square of the voltage swing. With the inductor inserted, the power consumption is reduced by at least 52% at 30 MHz. The maximum power saving occurs at 70 MHz and the amount is 72%. An important feature of the *LC* resonance buffer is that its power consumption does not depend on the operating frequency. This is because the power loss of the resonator is only related to its resistance and the signal swing. This property is quite beneficial to design of the high-speed BCC transceiver [5].

IV. Conclusion

This study has proposed a planar MICS band antenna combined with an electrode for BCC. The spiral microstrip antenna is designed to have 2.5×1.8 cm^2 size and 2-mm thickness, and hence, it can be attached to human skin conveniently. The resonant frequency of the on-body antenna is 400 MHz and the bandwidth is 36 MHz from the S_{11} measurements. The path-loss measurement inside the human phantom shows that the signal radiated from the proposed antenna attenuates with a -28-dB/m rate and the minimum power received by the implanted antenna is -75 dBm at 1.2-m distance. The propagation loss of the human body channel is investigated in 10–70-MHz

frequencies and 20–150-cm distances when the antenna is used as the electrode for BCC. Due to the protective layer on the radiating body of the antenna, the 6-dB channel loss is added. The electrical circuit modeling of the on-body antenna in the 25–100-MHz frequency indicates that the capacitance of the antenna increases >3 times due to the skin contact. To drive the large capacitive load of the antenna with low power consumption, the *LC* series resonance is utilized in the BCC TX buffer. As a result, the power saving of 50%–70% is achieved.

REFERENCES

[1] J. A. V. Arx and K. Najafi, "A wireless single-chip telemetry-powered neural stimulation system," in *IEEE Int. Solid-State Circuits Conf. Tech. Dig.*, Feb. 1999, pp. 214–215.

[2] FCC Rules and Regulations 47 CFR Part 95.

[3] P. D. Bradley, "An ultra low power, high performance medical implant communication system (MICS) transceiver for implantable devices," in *IEEE Biomed. Circuits Syst. Conf.*, Nov. 2006, pp. 158–162.

[4] A. Tekin, M. R. Yuce, and W. Liu, "A low power MICS band transceiver architecture for implantable devices," in *IEEE Wireless Microw. Tech. Conf.*, Apr. 2005, pp. 55–58.

[5] N. Cho, J. Bae, S. Kim, and H.-J. Yoo, "A 10.8 mW body-channel-communication/MICS dual-band transceiver for a unified body-sensor-network controller," in *IEEE Int. Solid-State Circuits Conf. Tech. Dig.*, Feb. 2009, pp. 424–425, 425a.

[6] B. W. Cook, A. Berny, A. Molnar, S. Lanzisera, and K. S. J. Pister, "Low-power 2.4-GHz transceiver with passive RX front-end and 400-mV supply," *IEEE J. Solid-State Circuits*, vol. 41, no. 12, pp. 2757–2766, Dec. 2006.

[7] J. L. Bohorquez, J. L. Dawson, and A. P. Chandrakasan, "A 350 μW CMOS MSK transmitter and 400 W OOK super-regenerative receiver for medical implant communications," in *IEEE VLSI Circuits Symp.*, Jun. 2008, pp. 32–33.

[8] N. Cho, J. Yoo, S.-J. Song, J. Lee, S. Jeon, and H.-J. Yoo, "The human body characteristics as a signal transmission medium for intrabody communication," *IEEE Trans. Microw. Theory Tech.*, vol. 55, no. 5, pp. 1080–1086, May 2007.

[9] S. J. Song *et al.*, "A 0.9 V 2.6 mW body-coupled scalable PHY transceiver for body sensor applications," in *IEEE Int. Solid-State Circuits Conf. Tech. Dig.*, Feb. 2007, pp. 366–367.

[10] P. Soontornpipit, C. M. Furse, and Y. C. Chung, "Design of implantable microstrip antenna for communication with medical implants," *IEEE Trans. Microw. Theory Tech.*, vol. 52, no. 8, pp. 1944–1951, Aug. 2004.

[11] J. Kim and Y. R. Samii, "Implanted antennas inside a human body: Simulations, designs, and characterizations," *IEEE Trans. Microw. Theory Tech.*, vol. 52, no. 8, pp. 1934–1943, Aug. 2004.

[12] "Application note 3401," Maxim, Dallas, TX, 2004. [Online]. Available: http://www.maxim-ic.com/an3401

[13] C. A. Balanis, *Antenna Theory: Analysis and Design*, 2nd ed. New York: Wiley, 1997.

[14] S. Gabriel and R. W. L. Gabriel, "The dielectric properties of biological tissues: II. Measurements in the frequency range 10 Hz to 20 GHz," *Phys. Med. Biol.*, pp. 2251–2269, Nov. 1996.

[15] K. Hachisuka, Y. Terauchi, Y. Kishi, K. Sasaki, T. Hirota, H. Hosaka, K. Fujii, M. Takahashi, and K. Ito, "Simplified circuit modeling and fabrication of intrabody communication devices," *Sens. Actuators A, Phys.*, vol. 130–131, pp. 322–330, Jun. 2006.

[16] M. Shinagawa, M. Fukumoto, K. Ochiai, and H. Kyuragi, "A near-field-sensing transceiver for intrabody communication based on the electrooptic effect," *IEEE Trans. Instrum. Meas.*, vol. 53, no. 12, pp. 1533–1538, Dec. 2004.

Namjun Cho (S'04) received the B.S. (*summa cum laude*) and M.S. degrees from the Korea Advanced Institute of Science and Technology (KAIST), Daejeon, Korea, in 2004 and 2006, respectively, and is currently working toward the Ph.D. degree at KAIST.

He has been involved with the development of UHF RF identification (RFID) tag chips integrated with environmental monitoring sensors and low-power digital-to-analog converters for hearing-aid systems. His current research interests include low-power biomedical microsystems and the wireless transceivers for body area networks.

Taehwan Roh (S'09) received the B.S. degree in electrical engineering and computer science from the Korea Advanced Institute of Science and Technology (KAIST), Daejeon, Korea, in 2009, and is currently working toward the M.S. degree in electrical engineering and computer science at KAIST.

His current research interests include high-speed frequency shift-keying (FSK) demodulation and baseband design for body sensor networks.

Joonsung Bae (S'07) received the B.S. and M.S. degrees in electrical engineering and computer science from the Korea Advanced Institute of Science and Technology (KAIST), Daejeon, Korea, in 2007 and 2009, respectively, and is currently working toward the Ph.D. degree in electrical engineering and computer science at KAIST.

He has been involved with the development of transceivers for high-speed on-chip global interconnects and the wireless CMOS transceivers for communicating among wearable and implantable devices. His current research interests include low-energy CMOS transceiver design for electric field communication.

Hoi-Jun Yoo (M'95–SM'04–F'08) received the Electronic degree from Seoul National University, Seoul, Korea, in 1983, and the M.S. and Ph.D. degrees in electrical engineering from the Korea Advanced Institute of Science and Technology (KAIST), Daejeon, Korea, in 1985 and 1988, respectively. His doctoral research concerned the fabrication process for GaAs vertical opto-electronic integrated circuits.

From 1988 to 1990, he was with Bell Communications Research, Red Bank, NJ, where he invented the 2-D phase-locked vertical cavity surface emitting laser (VCSEL) array, the front-surface-emitting laser, and the high-speed lateral HBT. In 1991, he became a Manager of the Dynamic Random Access Memory (DRAM) Design Group, Hyundai Electronics, and designed a family of fast-1 M DRAMs to 256-M synchronous DRAMs. In 1998, he joined the faculty of the Department of Electrical Engineering, KAIST, where he is currently a tenured Professor. From 2001 to 2005, he was the Director of the System Integration and IP Authoring Research Center (SIPAC), funded by the Korean Government to promote worldwide IP authoring and its system-on-chip (SOC) application. From 2003 to 2005, he was the Full-Time Advisor to the Minister of the Korea Ministry of Information and Communication and National Project Manager for SoCs and Computers. In 2007, he founded the System Design Innovation and Application Research Center (SDIA), KAIST, to research and develop SoCs for intelligent robots, wearable computers, and bio systems. His current interests are high-speed and low-power network on chips, 3-D graphics, body area networks, biomedical devices and circuits, and memory circuits and systems. He authored *DRAM Design* (Hongleung, 1996, in Korean), *High Performance DRAM* (Sigma, 1999, in Korean), *Low-Power NoC for High-Performance SoC Design* (CRC, 2008), and chapters of *Networks on Chips* (Morgan Kaufmann, 2006).

Dr. Yoo is an Executive Committee member and the Far East secretary for the IEEE International Solid-State Circuits Conference (ISSCC), and a Steering Committee member of the IEEE A-SSCC. He was the Technical Program Committee chair of A-SSCC 2008. He was the recipient of the 1994 Electronic Industrial Association of Korea Award for his contribution to DRAM technology, the 1995 Hynix Development Award, the 2001 Design Award of ASP-DAC, the 2002 Korea Semiconductor Industry Association Award, the 2007 KAIST Best Research Award, and the 2005–2007 Asian Solid-State Circuits Conference (A-SSCC) Outstanding Design Awards.